PCCP

RSC Publishing

PAPER

View Article Online
View Journal | View Issue

Efficient energy transfer from InGaN quantum wells to Ag nanoparticles

Cite this: *Phys. Chem. Chem. Phys.*, 2013, **15**, 3618

G. W. Shu,[a] C. H. Chiu,[b] L. T. Huang,[a] T. N. Lin,[a] C. C. Yang,[a] J. S. Wang,[a] C. T. Yuan,[a] J. L. Shen,*[a] H. C. Kuo,*[b] C. A. J. Lin,[c] W. H. Chang,[c] H. H. Wang,[d] H. I. Yeh,[d] W. H. Chan,[e] W. C. Fan[f] and W. C. Chou[f]

Received 2nd November 2012,
Accepted 16th January 2013

DOI: 10.1039/c3cp43894e

www.rsc.org/pccp

Nonradiative energy transfer from an InGaN quantum well to Ag nanoparticles is unambiguously demonstrated by the time-resolved photoluminescence. The distance dependence of the energy transfer rate is found to be proportional to $1/d^3$, in good agreement with the prediction of the dipole interaction calculated from the Joule losses in acceptors. The maximum energy-transfer efficiency of this energy transfer system can be as high as 83%.

1. Introduction

Förster resonance energy transfer (FRET), in which a fluorescent donor transfers energy *via* nonradiative dipole–dipole interaction to a fluorescent or nonfluorescent acceptor, has been of great interest over the past decades.[1,2] FRET occurs when there is appreciable overlap between the emission spectra of donors and the absorption spectra of acceptors, and its efficiency strongly depends on the distance of separation between donors and acceptors. Further, there is a strong dependence on spatial orientation of the involved dipoles in FRET. No FRET is expected in a configuration where the dipole moment of a donor is perpendicular to that of an acceptor. FRET has extensive applications in biomedical systems, materials science, and optoelectronics.[3–5] However, the application of FRET sometimes suffers from the nature of the dipole–dipole mechanism, which restricts the distance between donors and acceptors on the order of $\sim$10 nm. Beyond this distance, the energy transfer becomes too weak. An alternative energy transfer involving fluorophores near metal nanoparticles (NPs) has also been found to exhibit a FRET-like process.[6–8] The nonradiative transition due to energy transfer between fluorophores and metal NPs leads to a strong fluorescence quenching at a close proximity to the surface, referred to as the nanometal surface energy transfer (NSET).[6–8] NSET does not require a resonant electronic transition, which is fundamental to a FRET. Rather, it is associated with the interaction of the electromagnetic field of the donor dipole with the delocalized conduction electrons of the metal NP (acceptor). Factors affecting NSET include the physical and chemical characteristics of the fluorophores and metal NPs. NSET has been considerably studied because this technique is capable of measuring distance about twice as far as FRET, which help to understand the large scale conformational dynamics of complex biomolecules and to detect inorganic metal ions, viruses, and proteins.[9]

Recently, the development of donors and acceptors has focused on the use of nanomaterials as novel donors. Quantum dots, which provide remarkable optical properties, have been explored as the energy donors and a variety of quantum-dot-based energy-transfer sensors with high sensitivity have been implemented.[10–13] On the other hand, the semiconductor quantum wells (QWs) can also substitute for traditional organic fluorophores as the alternative energy donors.[14,15] Because of their size-tunable optical properties and excellent resistance to photobleaching and blinking, QWs are expected to be efficient donors in the energy transfer system. This suggests that QWs and metal NPs could provide good donor–acceptor pairs. The QW-based energy transfer is further motivated by the potential of incorporating it into on-chip nanostructures for applications in optoelectronic and biophotonic devices. In this study, we propose an energy-transfer system, in which the InGaN QW acts as the donor, the Ag NPs act as the acceptor, and the GaN cap layer acts as the spacer between the QW and the Ag NPs (Fig. 1(a)).

[a] *Physics Department, Chung Yuan Christian University, Chung-Li, Taiwan. E-mail: jlshen@cycu.edu.tw*
[b] *Department of Photonic and Institute of Electro-Optical Engineering, National Chiao Tung University, Hsin-chu, Taiwan. E-mail: hckuo@faculty.nctu.edu.tw*
[c] *Department of Biomedical Engineering, Chung Yuan Christian University, Chung-Li, Taiwan*
[d] *Department of Internal Medicine, Mackay Memorial Hospital, Mackay Medical College, New Taipei City, Taiwan*
[e] *Department of Bioscience Technology, Chung Yuan Christian University, Chung Li, Taiwan*
[f] *Department of Electrophysics, National Chiao Tung University, Hsin-chu 30010, Taiwan*

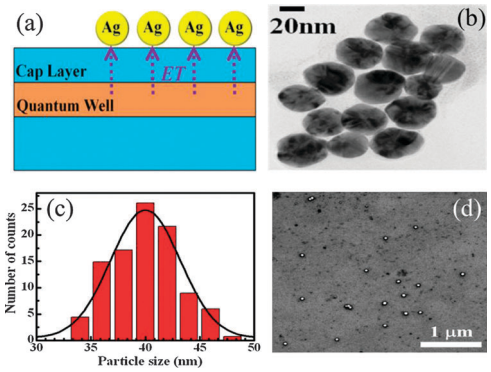

Fig. 1 (a) Schematic representation of the energy transfer system. The energy transfer from a quantum well (QW) to Ag nanoparticles (NPs) is marked by the dashed arrows. (b) A transmission electron microscopy (TEM) image of Ag NPs. (c) Particle size distribution obtained from TEM. The curve shows a Gaussian fit to the histograms. (d) A scanning electron microscopy image of Ag NPs on the surface of the QW.

Such energy transfer was investigated by the time-resolved photoluminescence (PL). Distance-dependent interactions of InGaN QWs with Ag NPs were studied to analyze the mechanism of energy transfer processes. A theoretical model based on the Joule loss of the electromagnetic field in the Ag NPs was used to calculate the energy transfer rate and the energy transfer efficiency. This new type of energy transfer could pave a way toward its potential applications for the development of nanosensors.

2. Experimental section

The donor used for the present study is a single InGaN/GaN QW structure grown by metal–organic chemical vapor deposition on a single-side polished (0001)-oriented sapphire substrate. After a 2 μm thick GaN buffer layer, a single InGaN QW layer with a thickness of 2 nm was grown on the substrate. The growth was terminated by the GaN cap layer with four different thicknesses to control the separation between donors and acceptors. At room temperature, the energy gap of the GaN cap layer was found to be as high as 3.452 eV.[16] Thus, the GaN cap layer cannot absorb the light emitted from the InGaN QW (photon energy = 3.062 eV), and it can thus act as a spacer between donors and acceptors. The cap-layer thicknesses of four samples used in this study were 2, 4, 6, and 8 nm. The acceptor in this study was the Ag NP with a citrate-stabilized surface at concentrations of 0.02 mg mL^{-1}, which was purchased from *Sigma-Aldrich*. To determine the size of Ag NPs, transmission electron microscope (TEM) measurements were performed. Fig. 1(b) shows the TEM image of the Ag NPs formed from droplets of the colloidal solution. The histograms of particle size distribution obtained by counting about 100 particles in the TEM images are shown in Fig. 1(c). The Ag NPs investigated are roughly uniform in size. The diameter size distribution was fitted to the Gaussian shape, which is shown by the solid line in Fig. 1(c). The average size of Ag NPs was found to be 40 ± 3 nm from the fit of the corresponding Gaussian shape.

To perform the energy transfer experiment, the Ag NPs were incorporated on the top of the QW cap layer by the drop-casting method upon evaporation of the solvent. Fig. 1(d) shows the scanning electron microscope (SEM) image of Ag NPs on the surface of the investigated InGaN QW. Basically, the Ag NPs are uniformly dispersed without aggregation.

The steady-state and time-resolved PL of the InGaN QW was measured at room temperature. A pulsed laser with a wavelength of 260 nm, a repetition frequency of 20 MHz, and a duration of 250 fs was used as the excitation source. The collected luminescence from the surface of the InGaN QW was projected into a spectrometer and detected using a high-speed photomultiplier tube (PMT). Time-resolved PL was performed using the technique of time-correlated single-photon counting (TCSPC). The instrument response of the time-correlated single photon counting system is about 250 ps.

3. Results and discussion

The open circles in Fig. 2 show the optical absorption spectrum of the Ag NPs. A strong absorption band due to surface plasmon resonance was observed at around 410 nm. This optical absorption can be fitted to obtain the dielectric constant of Ag NPs (ε), which will be used later. According to Drude free electron theory and the Lorentz oscillator model, ε can be represented by an analytic function:[17]

$$\varepsilon = 1 - \frac{{\omega_p}^2}{\omega^2 + i\gamma\omega} + \frac{a}{{\omega_0}^2 - \omega^2 - i\Gamma\omega} + \varepsilon_\infty, \qquad (1)$$

where ω_p is the plasma frequency, γ is the damping constant of plasma, a is the amplitude of interband transitions, Γ is the broadening term of interband transitions, ω_0 is the resonance energy of interband transitions, and ε_∞ is the dielectric constant at high frequencies compared to interband transitions. The dielectric function of the conduction electrons is represented by the first two terms, while the interband and all other non-Drude contributions are expressed by the last two terms. With ω_p = 9.868 eV, γ = 0.395 eV, ω_0 = 4.429 eV, a = 4.9 e^2 V^2, Γ = 0.658 eV, and ε_∞ = 2.3, the fits according to eqn (1) are displayed as the dashed line in Fig. 2. The fitted result is in

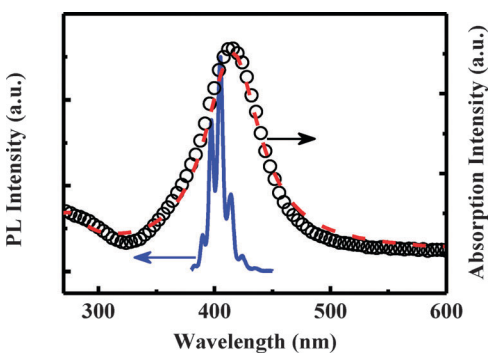

Fig. 2 Absorption spectrum of Ag NPs (open circles) and photoluminescence spectrum of the InGaN QW (solid line). The dashed line is the fitted curve using eqn (1).

good agreement with the measured optical absorption. This fit produces a value of $\varepsilon = -3.6 + 1.06i$ for Ag NPs at the resonance wavelength.

The solid line in Fig. 2 shows the PL spectrum of the InGaN QW with a cap thickness of 2 nm. The PL reveals a narrow PL band that peaks at around 405 nm. This wavelength is close to the spectral range of strong absorption (surface plasmon resonance) for Ag NPs, which allows strong coupling between the InGaN QW and the Ag NP. Thus, a pronounced spectral overlap between donor emission and acceptor absorption occurs. On the other hand, in the QW-based system, the donor's dipole moment is oriented in the direction of the QW plane and the acceptor's dipole moment has a random orientation.[18] With the above conditions and the proximal distance between the InGaN QW and the Ag NPs, the energy transfer in our system can be feasible.

To demonstrate the energy transfer between QWs and NPs, the PL decays of the bare QW and the hybrid structure (*i.e.*, QWs plus NPs) were measured. If the energy transfer is mediated through a nonradiative process, a decrease in the donor lifetime should be observed. Fig. 3 shows the PL decay curves of QWs without (open circles) and with (open triangles) the Ag NPs for four QWs with different cap thicknesses. Evidently, the presence of Ag NPs in all samples accelerates the QW PL decay, in agreement with the behavior of energy transfer from donors to acceptors. The PL decay of the InGaN QW is expected to be characterized by a distribution of lifetimes owing to the presence of spatial disorder or/and phase separation in InGaN materials. All the PL decay curves in Fig. 3 were thus fitted by the stretched exponential function:[19]

$$n(t) = n(0)\mathrm{e}^{-(kt)^{\beta}} \quad (2)$$

where $n(t)$ are carrier densities in donors and k is the decay rate of carriers in donors and β is a dispersive exponent. The solid lines in Fig. 3 show the fitted curves using eqn (2), consistent with the experimental data. In the stretched exponential function the average decay time is calculated as follows:[20]

$$\langle\tau\rangle = \frac{1}{k\beta}\Gamma\left(\frac{1}{\beta}\right), \quad (3)$$

where Γ is the mathematical gamma function.

According to the optical properties of QWs, the PL decay rate of the bare InGaN QW can be expressed as

$$\tau_{\mathrm{QW}}{}^{-1} = \tau_{\mathrm{R}}{}^{-1} + \tau_{\mathrm{NR}}{}^{-1}, \quad (4)$$

where τ_{QW} and τ_{NR} represent the radiative and nonradiative decay time of the bare QW, respectively. After introducing Ag NPs, the PL decay of the QW can be described by the following equation:

$$\tau_{\mathrm{hybrid}}{}^{-1} = \tau_{\mathrm{R}}{}^{-1} + \tau_{\mathrm{NR}}{}^{-1} + \tau_{\mathrm{ET}}{}^{-1} \quad (5)$$

where τ_{ET} represents the characteristic time of the energy transfer process. In Fig. 3, reduction of the QW lifetime after introducing the Ag NPs confirms the presence of an additional decay channel that we have previously assigned to energy transfer. The corresponding energy transfer rate can then be determined from $\tau_{\mathrm{hybird}}{}^{-1} - \tau_{\mathrm{QW}}{}^{-1}$. The open circles in Fig. 4 display the experimental energy transfer rate (K_{ET}) for the samples with four different cap thicknesses. Obviously, the energy transfer rate decreases monotonically with an increase in the cap thickness of InGaN QWs.

The energy transfer mechanism is strongly dependent on whether the electronic excitations are unbound carriers (free electrons and holes) or Coulombically bound electron–hole pairs (excitons).[14,15] For unbound carriers, the calculation of the dipole–dipole interaction expects an energy transfer rate that depends linearly on the carrier density.[14] For excitons, the energy transfer rate is independent of the density of excitons. Therefore, it is necessary to determine the type of electronic excitations in the QW before analyzing the energy transfer in our system. The excitation-density dependence of PL in the bare QW has been measured to find out the type of carrier. The open circles in Fig. 5 show the dependence of the PL intensity of InGaN QWs on excitation density. A least square fit of the experimental data is displayed as the solid line in Fig. 5, revealing a slope value of 1.9. Such linear scaling suggests that the carriers in our InGaN QW are in the form of unbound electrons and holes, indicating that the energy transfer rate should also scale linearly with carrier density.[15]

The energy transfer rate from InGaN QWs to Ag NPs was calculated based on a semiclassical approach, which considers a microscopic quantum well model with a macroscopic

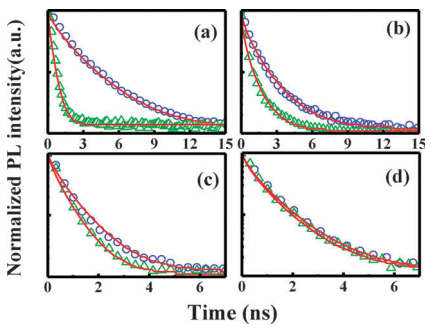

Fig. 3 The PL decay profiles of the InGaN QW in the absence (open circles) and presence (open triangles) of Ag NPs with a cap thickness of (a) 2 nm, (b) 4 nm, (c) 6 nm, and (d) 8 nm. The solid lines are the fitted curves using eqn (2).

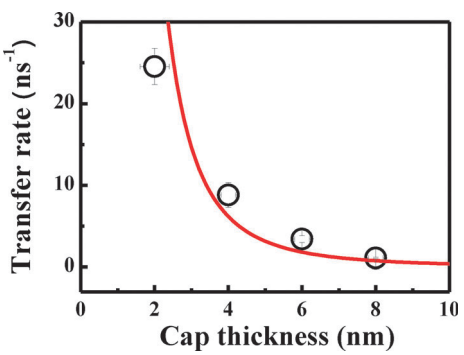

Fig. 4 The dependence of the measured energy transfer rate on the cap thickness (open circles). The solid line is the fit curve using eqn (6).

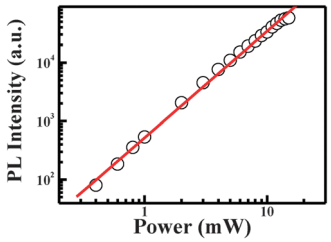

Fig. 5 The dependence of the PL intensity in the InGaN QW on excitation density. The nearly quadratic dependence reveals that recombination is dominated by unbound electron–hole pairs.

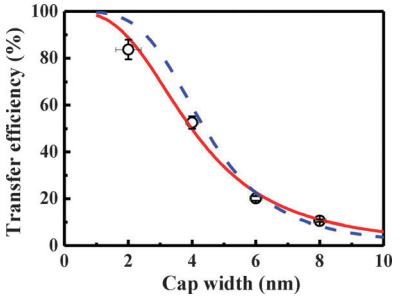

Fig. 6 The dependence of the measured energy transfer efficiency on the cap thickness (open circles). The solid and dashed lines are the fit curves using eqn (8) and (9), respectively.

electrodynamical description.[14] In this model, the nonradiative energy transfer rate due to the dipole–dipole interaction can be calculated from the Joule losses of the electromagnetic field in the acceptor materials.[14] These are produced by the penetration into the acceptors of the electric field generated by the polarization of the QW excitations, which is proportional to the imaginary part of the dielectric function in acceptors. According to the model in ref. 14, we can estimate the energy transfer rate K_{ET} taking into consideration the unbound carriers by the following expression:

$$K_{ET}(L_b) = A\frac{n_e n_h}{h}\frac{\mathrm{Im}\,\varepsilon}{|\varepsilon+\varepsilon_b|^2}\frac{|d_{vc}|^2 {L_T}^2}{{L_b}^3}, \quad (6)$$

where A is a numerical factor, n_e (n_h) is the two-dimensional electron (hole) densities in the system, h is the Planck constant, d_{vc} is the electric dipole transition moment, ε_b is the semiconductor background dielectric constant, and L_b is the cap thickness. L_T is the thermal length and defined by[14]

$${L_T}^2 = \frac{\hbar^2}{2(m_e+m_h)T}, \quad (7)$$

where m_e and m_h are the effective mass of electrons and holes in the QW, respectively.

By taking $\varepsilon_b = 6.25$, $\varepsilon = -3.6 + 1.06i$, $n_e = n_h = 3 \times 10^{12}$ cm^{-2}, $A \sim 1.23$, $m_e = 0.2m_0$, $m_h = 0.8m_0$, $T = 300$ K, and $d_{vc} = 14$ Debye, we can obtain the energy transfer rate as a function of the cap thickness. The solid line in Fig. 4 shows the curve of the calculated energy transfer rate according to eqn (6) and (7). It can be seen that the calculated results agree with the experimental data. This indicates that the energy transfer from the InGaN QW to the Ag NC can be explained by the above model. For the 2 nm-cap sample, the calculation deviates from the experimental result. This discrepancy probably originates from the monolayer thickness fluctuations in that sample, leading to local carrier accumulation and affecting the energy transfer rate.[21]

The energy-transfer efficiency is the fraction of the photons absorbed by the donor that are transferred to the acceptor and can be described by

$$\Phi_{ET} = \frac{K_{ET}}{{\tau_{QW}}^{-1} + K_{ET}}. \quad (8)$$

Taking $\tau_{ET} = 1.6$ ns, the experimental energy-transfer efficiency for four samples can thus be obtained, displayed as the open circles in Fig. 6. A descending trend of the energy-transfer efficiency was observed as the cap thickness increases. The maximum energy transfer efficiency obtained from experiment is as high as 83% for the InGaN QW with a cap thickness of 2 nm. The high energy transfer efficiency in this system indicates a higher signal-to-background ratio and thus better sensitivity and a greater dynamic range for the applicability in biological sensing. The theoretical plot of the energy transfer efficiency as a function of the cap thickness was also estimated using eqn (6)–(8), displayed as the solid line in Fig. 6. This theoretical modeling fits quite well with measured data.

For the interaction between fluorophores and proximal metal nanoparticles, an alternative model NEST, which describes that the energy transfer efficiency has a distance dependence of $1/d^4$, has been reported.[6,10,22] In order to check whether the mechanism of energy transfer in our system is NSET, the energy transfer efficiency of NEST was calculated. The empirical distance dependence of the energy transfer efficiency in NEST can be expressed as:[22]

$$\Phi_{NEST} = \frac{1}{1+(d/d_0)^4}, \quad (9)$$

where d is the distance between donors and acceptors and d_0 is the donor-to-acceptor distance at which the energy transfer efficiency is 50%. With $d_0 = 4.4$ nm, the fit according to eqn (9) is displayed as a dashed line in Fig. 6. It is found that the model based on the Joule losses in acceptors provides a better fit to the data than NSET. This implies that the energy transfer efficiency in our system follows a $1/d^3$ distance dependence since the energy transfer rate in eqn (6) is proportional to ${L_b}^{-3}$. The $1/d^3$ distance dependence has also been reported for the energy transfer from a two-dimensional donor layer to a three-dimensional array of acceptors.[23] In the NSET mechanism, the interaction between a donor and an acceptor corresponds to a point dipole and an infinite metal surface, respectively. In the present case, the donor is a two-dimensional QW, not a point dipole. Thus, NSET may have the deviation for describing the energy transfer between QWs and proximal Ag NPs. However, we cannot completely rule out the possibility that NSET contributes to the energy transfer in our system. According to the result in Fig. 6, the NSET model can roughly explain the distance dependence of the energy transfer efficiency.

4. Conclusions

We have demonstrated an energy transfer from InGaN QWs to Ag NPs by observing a shortening of the PL decay time for the InGaN QW in the presence of Ag NPs. Upon increasing the separation between QWs and NPs, the energy transfer rate and efficiency decrease rapidly, following a $1/d^3$ distance dependence. These results are well matched with the electrodynamics model by considering the dipole–dipole interaction calculated from the Joule losses in the acceptor. The transfer efficiency obtained from the time-resolved PL is as high as 83% for the QW with a cap thickness of 2 nm. Such highly efficient energy transfer may be promising for developing sensing applications.

Acknowledgements

This project was supported in part by the National Science Council under the grant numbers NSC 100-2112-M-033-005-MY3 and NSC101-2627-M-033-002.

References

1 T. Förster, *Ann. Phys.*, 1948, **2**, 55–75.
2 J. R. Lakowicz, *Principle of Fluorescence Spectroscopy*, Kluwer Academic Plenum, New York, 2nd edn, 1999.
3 G. A. Quiñones, S. C. Miller, S. Bhattacharyya, D. Sobek and J. P. Stephan, *J. Cell. Biochem.*, 2012, **113**, 2397–2405.
4 V. M. Agranovich, Y. N. Gartstein and M. Litinskaya, *Chem. Rev.*, 2011, **111**, 5179–5214.
5 G. Itskos, C. R. Belton, G. Heliotis, I. M. Watson, M. D. Dawson, R. Murray and D. D. C. Bradley, *Nanotechnology*, 2009, **20**, 275207.
6 C. S. Yun, A. Javier, T. Jennings, M. Fisher, S. Hira, S. Peterson, B. Hopkins, N. O. Reich and G. F. Strouse, *J. Am. Chem. Soc.*, 2005, **127**, 3115–3119.
7 R. Chhabra, J. Sharma, H. Wang, S. Zou, S. Lin, H. Yan, S. Lindsay and Y. Liu, *Nanotechnology*, 2009, **20**, 485201.
8 J. Ling and C. Z. Huang, *Anal. Methods*, 2010, **2**, 1439–1447.
9 Y. Chen, M. B. O'Donoghue, Y. Huang, H. Kang, J. A. Phillips, X. Chen, M. C. Estevez, C. J. Yang and W. Tan, *J. Am. Chem. Soc.*, 2010, **132**, 16559–16570.
10 T. Pons, I. L. Medintz, K. E. Sapsford, S. Higashiya, A. F. Grimes, D. S. English and H. Matoussi, *Nano Lett.*, 2007, **7**, 3157–3164.
11 A. Jaiswal, P. Sanpui, A. Chattopadhyay and S. G. Siddhartha, *Plasmonics*, 2011, **6**, 125–132.
12 M. Li, S. K. Cushing, Q. Wang, X. Shi, L. A. Hornak, Z. Hong and N. Wu, *J. Phys. Chem. Lett.*, 2011, **2**, 2125–2129.
13 K. K. Haldar, T. Sen and A. Patra, *J. Phys. Chem. C*, 2010, **114**, 4869–4874.
14 D. Basko, G. C. La Rocca, F. Bassani and V. M. Agranovich, *Eur. Phys. J. B*, 1999, **8**, 353–362.
15 M. Achermann, M. A. Petruska, S. Kos, D. L. Smith, D. D. Koleske and V. I. Klimov, *Nature*, 2004, **429**, 642–664.
16 J. F. Muth, J. H. Lee, I. K. Shmagin, R. M. Kolbas, H. C. Casey Jr, B. P. Keller, U. K. Mishra and S. P. DenBaars, *Appl. Phys. Lett.*, 1997, **71**, 2572–2574.
17 M. Moskovits, I. Srnová-Šloufová and B. Vlčková, *J. Chem. Phys.*, 2002, **116**, 10435.
18 Š. Kos, M. Achermann, V. I. Klimov and D. L. Smith, *Phys. Rev. B: Condens. Matter Mater. Phys.*, 2005, **71**, 205309.
19 M. Pophristic, F. H. Long, C. Tran, I. T. Ferguson and R. F. Karlicek Jr, *J. Appl. Phys.*, 1999, **86**, 1114–1118.
20 A. F. van Driel, I. S. Nikolaev, P. Vergeer, D. Vanmaekelbergh and W. L. Vos, *Phys. Rev. B: Condens. Matter Mater. Phys.*, 2007, **75**, 035329.
21 X. Zhou, E. T. Yu, D. Florescu, J. C. Ramer, D. S. Lee and E. A. Armour, *Appl. Phys. Lett.*, 2004, **85**, 407–409.
22 S. Saraswat, A. Desireddy, D. Zheng, L. Guo, H. P. Lu, T. P. Bigioni and D. Isailovic, *J. Phys. Chem. C*, 2011, **115**, 17587–17593.
23 D. R. Haynes, A. Tokmakoff and S. M. George, *J. Chem. Phys.*, 1994, **100**, 1968–1980.

